# A Lower Bound on the Quark Matching Scale in VERSF

*Source dynamics, metric dependence and weak response*

Keith Taylor
28 November 2026

## General reader summary

An earlier VERSF paper showed how a quark's interaction with a source that stores its history can change the calculated chances of one quark turning into another. Here we calculate how that source moves and ask how small its energy scale can be before the same interaction changes quark masses too strongly or exceeds limits from neutral mesons.

With one choice for how the model measures a change in the quark coupling, all six versions pass the stated tests above about 0.94 trillion electron volts. Raising the energy weakens the effects being tested and leaves the original mixing pattern unchanged. The calculation therefore gives a lower bound and leaves the upper end open. Most of the mass response comes from an interaction shared by all six flavours. A second choice of how to measure the coupling makes that response too large at every energy allowed by the flavour tests.

A separate calculation asks whether supplying the same energy to a cell always produces the same weak response. Two operations that supply equal energy give different answers, even at the weaker coupling used for the mass calculation. Which operation is applied, and when, matters. What sets the rate of such events in nature remains open.

## Abstract

Starting from the history-mediator action [1], we recover its static energy and derive a finite source dynamics with inertia $m_s=18391/86955$. Its spectral covariance fixes the connected response. We project the scalar interaction onto neutral-meson operators and calculate first-order pole-mass and temporal-current derivatives with both external-state and vertex terms. At fixed Yukawa seed, canonical conversion and unit completion metric on T, the largest of the six ten-percent mass-budget crossings is $E_0=0.939082$ TeV. The largest historical flavour crossing is 0.928792 TeV. The tests impose a lower bound and supply no upper bound. At 1 TeV the maximum mass derivative is 8.8201%, of which 6.8893 percentage points come from the identity contact. The relative us/ud current-ratio derivative has magnitude below 0.001153. Assigning the unit metric to $X_H=\kappa_H T_H$ leaves this current and the neutral-flavour projections unchanged, but gives fractional mass derivatives of 2.26–2.29 at 1 TeV and fails the mass budget throughout the flavour-allowed range. In a separate finite cell, equal-work recording operations give distinct responses at both $\kappa_H=1$ and 0.174103600. These are conditional first-order and finite-cell results. A physical metric, retarded matching and a joint flavour fit remain open.

# Contents

1 The result and its relation to the published construction 3
2 A dynamic completion of the inherited source 3
3 Quantum motion and fluctuations counted once 5
4 Neutral mesons and lower bounds on the matching scale 6
5 The flavour preserving contact and metric dependence 8
6 Pole masses and the weak vertex in one regulator 9
7 The lower bound across all six attachments 10
8 Recording during the same finite dynamics 12
9 From a cell response to a physical particle 14
10 What this adds to the Standard Model derivation 15
Appendix A Numerical conventions and independent checks 16
Appendix B Reproduction and source provenance 17
References 17

# Notation

**Table 1. Symbols used in this paper.**

| Symbol | Meaning | Status |
|---|---|---|
| $w=u+iv$; $z$ | Responsive source; fixed prepared source $z=1$ | Dimensionless construction coordinates |
| $m_s$; $\Delta_n$ | Source inertia; excitation gaps | Ordering-coordinate quantities |
| $\vartheta$; $\Omega$ | One of six attachments; inherited family rotation | Declared attachment and fixed seed |
| $K_h$; $C_F(\omega)$ | Mediator contact; connected source response | Eliminated and propagating parts |
| $\kappa_H$; $E_0$; $\varphi_H$ | Higgs-to-cell ratio; cell energy; calibrated Higgs amplitude | $\kappa_H=\varphi_H/E_0$ under declared matching |
| $\varepsilon_I$ | Multiplier of the instantaneous interaction | Mass and current derivatives are at $\varepsilon_I=0$ |
| $R_{us/ud}$ | Squared ratio of temporal us and ud current elements | Bulk response diagnostic |
| $P_{probe}$; $\mathcal{R}$ | Weak-probe probability and its leading coefficient | Finite recorded-cell response |
| $J_W$; $J$ | Temporal weak-current operator; CKM CP invariant | Distinct current and mixing quantities |
| $W_{inj,E}$ | Energy-dependent injection into the full state space | Includes eliminated configurations |
| $C_2$, $\tilde{C}_2$, $C_4$ | Physical scalar flavour-changing coefficients | Specified tree matching and QCD convention |

# 1 The result and its relation to the published construction

The numerical question is how low the cell matching energy $E_0$ can be for the six inherited attachments. With the unit metric on T and a fixed seed, the ten-percent pole-mass derivative budget gives $E_0 \gtrsim 0.9391$ TeV. The largest separate historical flavour crossing is 0.9288 TeV. Table 8 evaluates all six attachments at the round reference of 1 TeV. Raising $E_0$ suppresses the diagnostics while preserving the leading mixing matrix. There is no upper crossing that would select a preferred scale. A unit metric on $X_H$ changes the conclusion for the masses (Sections 5 and 7).

The published paper A History Mediator for Quark Mixing in VERSF [1] already supplies the stationary construction, its unit-inertia quantum matching, all six attachments, the complete mixed second-order kernel and the right-handed spurion argument for multiplicative mass corrections. Those results are not rederived or counted again as contributions here. Its Section 8 leaves source inertia, physical normalisation and the dressed current as requirements for a physical installation. This paper evaluates specified parts of that return and adds the independent flavour constraints that the same interaction must satisfy.

**Table 2. Relation to the published mediator paper [1].**

| Object | Established in [1] | Return in this paper |
|---|---|---|
| Stationary and unit-inertia mixing | Conditional mixing improvement and six-attachment spread | Used as the inherited construction |
| Source motion | Inertia scanned; physical metric left open | Explicit residual completion, induced inertia and spectral covariance |
| Generated interactions | Mixed contact and multiplicative mass protection | Complete scalar neutral-meson projection and scale diagnostics |
| Mass and weak response | Finite and bulk benchmarks at specified inputs | Lower bound from mass slopes and light-current response |
| Recording during propagation | A remaining physical attachment | Completed finite Fock channel, timing response and equal-work controls |

The November ledger [2] calls for one finite construction to face independent force and flavour tests with its inputs and observable conversion accounted for. This paper advances the flavour side of that programme. It does not calculate gauge strengths, establish physical colour confinement or revise the ledger's percentage assessment. The construction is well posed and uses the common residual forms [3–5]; identifying its finite carrier and weights with the fully selected primitive physical carrier remains a separate requirement. Existence of one compatible realisation is sufficient; uniqueness is not demanded.

Status convention. Exact statements refer to the displayed finite construction. Quantum matching is the leading effective-action average on its specified auxiliary branch. The bulk response is a derivative at zero instantaneous interaction multiplier. The meson scales use historical comparisons under an explicit canonical conversion, with the dimensionless seed held fixed. Numerical convergence controls implementation error and does not replace model, matching or experimental uncertainty. These conventions apply throughout.

# 2 A dynamic completion of the inherited source

## 2.1 Fixed inputs and the source slice

Let $D_u$ and $D_d$ be the diagonal inherited Yukawa singular values of [1, Eqs. (2)–(3)], and $\Omega$ its anti-Hermitian orientation with a=9/40, b=81/2000, c=243/100000 and phase $2\pi/3$. All numerical inputs are supplied in the calculation package; no mass or mixing centre is used to choose an attachment or forward coefficient.

The three pair coordinates are ordered (12,23,31), and $q=(1,\exp(-2\pi i/3),\exp(2\pi i/3))/\sqrt{3}$. The phase $e^{i\vartheta}q$ defines the six attachments $\vartheta=0,60,\dots,300$ degrees. Their common source spectrum does not select one of them.

$$\mathbb{H}(h)=\Sigma_{(ij)}(h_{ij}E_{ij}+h_{ij}^{*}E_{ji}),\quad Y_{u,d}(h)=\exp[i\mathbb{H}(h)\mp\Omega/2]D_{u,d}. \tag{1}$$

Write $z=x+iy$ and $w=u+iv$. On each of three wheel copies put $\theta_j=\pi j/3$ and $\rho_j=1+[x\cos\theta_j+y\sin\theta_j+u\cos(2\theta_j)+v\sin(2\theta_j)]/3$ on the six rim sites, leaving the hub perturbation zero. The four real embedding columns are orthonormal across the three copies. The source potential inherited from [1] is

$$\Gamma_s(z,w)=(3/4)\Sigma_{j=0}^{5}(\rho_j^2-1)^2+(2/3)|z|^2+(8/5)|w|^2. \tag{2}$$

The prepared slice is $z=1$; the other primitive coordinates are held fixed. The mediator energy is $W\|h-wq/\sqrt{2}\|^2+g\|C_\Delta^{\dagger}h\|^2$, with $W=75/434$, $g=8/93$ and $C_\Delta$ the directed triangle incidence. At rest its elimination gives $r_h=75/187$ and an extra source cost $d_h|w|^2/2$, with $d_h=4200/40579$. The completion coordinates are algebraic, with unit cost. Their static elimination and the stationary mixing return are established inputs from [1].

## 2.2 The radial metric and its exact static recovery

The current-constitutive and continuity residuals of the common action [3, Sections 17–21] provide a concrete dynamic completion. Let $D_W$ be the three-copy wheel incidence, $L_W=D_W^{\dagger}D_W$, and a prime differentiation with respect to ordering coordinate $\sigma$. At flat transport and unit residual weights, take

$$\Gamma_{rad}=\int d\sigma\,\{V(\rho)+(1/2)\|j-D_W\rho\|^2+(1/2)\|\rho'+D_W^{\dagger}j\|^2\}. \tag{3}$$

Here $V(\rho)=(1/4)\Sigma_{copy,j}(\rho_j^2-1)^2$; the three identical rim copies recover the first term of (2). The positive history action defines the Euclidean ordering continuation used for the source spectrum.

$$j_{*}=(I+D_WD_W^{\dagger})^{-1}D_W(\rho-\rho'),\quad M_\rho=(I+L_W)^{-1}. \tag{4}$$

$$\Gamma_{rad,red}=\int d\sigma\,\{V(\rho)+(1/2)(\rho'+L_W\rho)^{\dagger}M_\rho(\rho'+L_W\rho)\}. \tag{5}$$

Proposition 1. On this fixed flat branch, eliminating the full current gives the metric $M_\rho$. On the four-column source embedding E, the metric is $\mathrm{diag}(1/3,1/3,1/5,1/5)$, and the static current contribution is exactly $(2/3)|z|^2+(8/5)|w|^2$. Thus the responsive w mode has inertia 1/5 while recovering the original static source energy.

Proof. Completing the current square gives (4) and (5). The first and second wheel harmonics have Laplacian eigenvalues 2 and 4, so their metric eigenvalues are $1/(1+2)$ and $1/(1+4)$. Their static coefficients are $\ell^2/[2(1+\ell)]$. Since $M_\rho$ commutes with $L_W$, the mixed term is the endpoint derivative $(1/2)\partial_\sigma(\rho^{\dagger}M_\rho L_W\rho)$. Fixed endpoints, periodic histories or the corresponding endpoint transformation remove it. The Gaussian determinant is constant on this branch. ▫

The weight dependence matters. For residual weights $w_J,w_T$ and constitutive coefficient $\kappa$, the same calculation gives $m_\ell=w_Jw_T/(w_J+w_T\ell)$ and static current coefficient $m_\ell\kappa^2\ell^2/2$ [5, Proposition 13]. The six-defect reference $w_J=1/2,w_T=1/4$ therefore gives a different metric and static stiffness. The unit-weight completion here is chosen to recover (2); it is not silently substituted for that other benchmark. Additional physical cross blocks or direct inertias could alter the result.

## 2.3 The triangle current and the matter attachment

Set $a_\Delta=q/\sqrt{2}$ and $R_\Delta=C_\Delta^{\dagger}a_\Delta/3$. Since q is mean zero, $C_\Delta R_\Delta=a_\Delta$ and $\|R_\Delta\|^2=1/6$. Put the radial and triangle residuals in orthogonal slots of one declared positive residual carrier. The triangle extension is

$$\Gamma_\Delta=\int d\sigma\,\{W\|h-a_\Delta w\|^2+g\|R_\Delta w'+C_\Delta^{\dagger}h\|^2\}. \tag{6}$$

$$h_{*}=a_\Delta(r_hw-\beta_\Delta w'),\quad \beta_\Delta=112/561,\quad \Gamma_{\Delta,red}=\int d\sigma\,(m_\Delta/2)|w'+3w|^2. \tag{7}$$

$$m_\Delta=200/17391=d_h/9,\quad m_s=1/5+m_\Delta=18391/86955=0.2115002013. \tag{8}$$

With $A_\Delta=WI+gC_\Delta C_\Delta^\dagger$, the stationary equation is $A_\Delta h=Wa_\Delta w-gC_\Delta R_\Delta w'$ and $A_\Delta a_\Delta=(W+3g)a_\Delta$. Substitution proves (7). Its mixed term is again a total derivative; its static cost is $d_h|w|^2/2$. Both the source potential and its motion have therefore been returned by this completion, rather than assigning a kinetic coefficient after evaluating the spectrum.

Matter is attached to the shifted drift variable $h_{dr}=h+\beta_\Delta a_\Delta w'$. Completing the square gives $(h_{dr}-r_h a_\Delta w)^\dagger A_\Delta(h_{dr}-r_h a_\Delta w)+(m_\Delta/2)|w'+3w|^2$. This affine change has unit Jacobian at fixed source history and preserves the inherited static readout. It is a declared constitutive attachment. A coupling to the raw current instead carries $r_h-i\beta_\Delta\omega$ in frequency space and has different moving responses despite the same static energy. This calculation establishes one compatible finite residual construction, not a physical selection theorem for that attachment.

# 3 Quantum motion and fluctuations counted once

Canonical quantisation of the two real source coordinates, in ordering units with action quantum one, gives the confining operator below. The original unit-inertia result is not reused with a relabelled energy scale: the wavefunction and all averages are recalculated at $m_s$.

$$H_b=-(\partial_u^2+\partial_v^2)/(2m_s)+\Gamma_s(1,w)+d_h|w|^2/2. \tag{9}$$

The first gap is 5.130994190; the mean is $\langle u\rangle=-0.0883219415$, $\langle v\rangle=0$. The variances are 0.460036490 and 0.459765734. Hermite cutoffs 24 and 32 reproduce the gap within $10^{-10}$. These are properties of the specified source Hamiltonian, not measured particle energies. Its positive, nondegenerate ground state supplies the law used in every leading source average below.

$$C_{ij}(\sigma)=\Sigma_{n>0}a_{ni}^*a_{nj}\exp(-\Delta_n|\sigma|),\quad \hat{C}_{ij}(\omega)=\Sigma_{n>0}2\Delta_n a_{ni}^*a_{nj}/(\Delta_n^2+\omega^2). \tag{10}$$

Equation (10) is the Euclidean ground-state correlation and its Euclidean frequency transform. The real-time ordered-unit correlation for $t>0$ is $C_{ij}^>(t)=\Sigma_{n>0}a_{ni}^*a_{nj}\exp(-i\Delta_n t)$. Thus the exponential decay in the Euclidean table is not a physical dissipation or event rate. Real-time propagation in Section 8 uses the unitary group of the same Hamiltonian.

Here $a_{ni}=\langle n|w_i|0\rangle$ and $\Delta_n=E_n-E_{0,source}$. Reflection makes the off-diagonal entries vanish. The zero-frequency diagonal values are 0.179180524 and 0.178977808. The full spectral sums, rather than a separately postulated Gaussian noise, determine the time dependence.

**Table 3. Connected source covariance in ordering units.**

| $\lvert\sigma\rvert$ | $C_{11}$ | $C_{22}$ |
|---|---|---|
| 0.0 | 0.460036490 | 0.459765734 |
| 0.1 | 0.275226355 | 0.274983978 |
| 0.25 | 0.127416266 | 0.127251550 |
| 0.5 | 0.035318681 | 0.035249874 |
| 1.0 | 0.002715051 | 0.002706290 |

Let $F(w)$ collect the 36 real and imaginary entries of $Y_{u,d}(r_h a_\Delta w)$, and let $J_h$ be its derivative with respect to $\xi_h=\sqrt{2}(\mathrm{Re}\,h,\mathrm{Im}\,h)$. Denote by $A_R$ the real representation of $A_\Delta$. The local mediator contact and connected source kernel are

$$K_h=\langle J_h A_R^{-1} J_h^T\rangle,\quad C_F(\omega)=\Sigma_{n>0}2\Delta_n f_n f_n^T/(\Delta_n^2+\omega^2),\quad f_n=\langle 0|F|n\rangle. \tag{11}$$

$$K_{ct}=\nu_T^{-1}I_{36}+K_h,\quad K_{full}(\omega)=K_{ct}+C_F(\omega). \tag{12}$$

At the zero-degree attachment and $\nu_T=1$ the traces are 36, 6.5075671855 and 0.0174893905 for the identity, mediator and static connected-source pieces. Their total is 42.5250565761. The largest total eigenvalue is 3.177826563 and the smallest is one. All three pieces arise from the same source and completion construction. $C_F$ is used once after the source is eliminated; it is omitted as a separate contact when the source is propagated explicitly. The instantaneous loop calculation in Section 6 uses $K_{ct}$ and leaves the retarded-source loop open.

The changed source metric also changes the leading matched matrices $\bar{Y}_f=\langle Y_f\rangle$. The results below are a consequence of the dynamic completion, not a new claim for the stationary mechanism in [1]. The inherited signed convention is $J=\mathrm{Im}(V_{ud}V_{cs}V_{us}^{*}V_{cd}^{*})$; conjugating the complete attachment reverses it. All six choices are shown because the source spectrum does not choose the favourable one.

**Table 4. Leading matched mixing at the derived inertia. These are not complete dressed physical CKM predictions.**

| $\vartheta$ | $\lvert V_{us}\rvert$ | $\lvert V_{ub}\rvert$ | $\lvert V_{cb}\rvert$ | $\lvert V_{td}\rvert$ | $10^5J$ |
|---|---|---|---|---|---|
| 0° | 0.2246790 | 0.0030670 | 0.0426947 | 0.0083947 | -2.425617 |
| 60° | 0.2249787 | 0.0014301 | 0.0413225 | 0.0081233 | -0.650523 |
| 120° | 0.2252149 | 0.0025150 | 0.0397438 | 0.0065318 | 0.288905 |
| 180° | 0.2251588 | 0.0042129 | 0.0395951 | 0.0048412 | -0.310502 |
| 240° | 0.2249058 | 0.0051736 | 0.0410282 | 0.0050959 | -1.931245 |
| 300° | 0.2246652 | 0.0047644 | 0.0425259 | 0.0070239 | -3.093530 |

At zero degrees the inherited $\lvert V_{td}\rvert$ and $\lvert J\rvert$ discrepancies shrink by 92.5% and 45.6%, while $\lvert V_{ub}\rvert$ worsens. At 300 degrees the magnitude of J is close to its reference, but the other entries do not all agree. The mass-retention factors have a common decrease of approximately 2.43%, with relative shape change below 16 parts per million before the additional interactions. Neither these percentages nor the change from the unit-inertia branch select an attachment. The fixed PDG comparison and its CP convention are those of [1,6,8].

# 4 Neutral mesons and lower bounds on the matching scale

## 4.1 The complete scalar projection

A history coupling between quark families also generates neutral flavour-changing contacts. These are an independent consequence of the same kernel that modifies charged mixing. Write $\bar{Y}_f=L_f\bar{d}_fR_f^{\dagger}$, with ascending singular values. For a real completion basis $E_a$, consisting of $E_{ij}$ and $iE_{ij}$ in each factor, define $v_a=(L_f^{\dagger}E_aR_f)_{ij}^{*}$ and $t_a=(L_f^{\dagger}E_aR_f)_{ji}$, with i lighter than j. The tree scalar coefficients in the conventional $\Delta F=2$ basis [9] are

$$Q_2=(\bar{q}_{jR}^{\alpha}q_{iL}^{\alpha})(\bar{q}_{jR}^{\beta}q_{iL}^{\beta}),\quad \tilde{Q}_2=(\bar{q}_{jL}^{\alpha}q_{iR}^{\alpha})(\bar{q}_{jL}^{\beta}q_{iR}^{\beta}), \tag{13}$$

$$Q_4=(\bar{q}_{jR}^{\alpha}q_{iL}^{\alpha})(\bar{q}_{jL}^{\beta}q_{iR}^{\beta}),\quad H_{\Delta F=2}=\Sigma_iC_iQ_i+\mathrm{h.c.} \tag{14}$$

$$c_2=-v^{T}Kv/2,\quad \tilde{c}_2=-t^{T}Kt/2,\quad c_4=-v^{T}Kt,\quad K=K_h+C_F(0). \tag{15}$$

The transposes in (15) are not Hermitian contractions. Both colour indices are independently summed. The vector operator and colour-exchanged scalar operators have zero tree coefficients in this matching, although QCD evolution generates the latter. The static source response is justified here only below its excitation scale. All coefficients, including relative phases, are retained; a small light-quark projection does not bound the bottom-changing contact.

Proposition 2. The identity completion contact gives zero coefficients in (15) for i≠j in every unitary mass frame. The mediator also gives zero at Ω=0,h=0, and after averaging the unprepared z=0 source ground state at Ω=0. These statements do not remove the flavour-preserving contact or the rotated and displaced mediator.

Proof. Real and imaginary matrix units cancel $v^{T}v$ and $t^{T}t$. Their cross contraction is twice the Hilbert–Schmidt inner product of distinct transformed matrix units and vanishes by unitarity. At the symmetric mediator point the proper complex covariance satisfies $\langle \delta h\, \delta h^{T}\rangle=0$; the flavour-changing squares carry two units of its phase charge. For the unprepared quantum source use the exact threefold symmetry, not a continuous symmetry of the nonlinear exponential: w,h acquire exp(2πi/3), and ℍ is conjugated by diag(1,exp(−2πi/3),exp(−4πi/3)). The ground state preserves that symmetry, while each ΔF=2 operator has nonzero charge modulo three. Its average is therefore zero. ▫

Random-frame checks of the identity contact are below $2.5\times10^{-16}$; the symmetric unprepared quantum residual is below $4.6\times10^{-19}$. The theorem is applied before multiplying by dimensionful scale factors. For kaon CP comparisons the phase of $\lambda_u=V_{us}^{*}V_{ud}$ is removed from the coefficients by $\exp[-2i\arg(\lambda_u)]$. This eliminates arbitrary SVD phase choices. A full conjugate attachment reverses the imaginary parts but leaves the absolute diagnostics below unchanged.

**Table 5. Dimensionless coefficients at zero degrees and the derived inertia, with the connected source counted once.**

| Channel | $\lvert c_2\rvert$ | $\lvert \tilde{c}_2\rvert$ | $\lvert c_4\rvert$ |
|---|---|---|---|
| K | 1.14897e-09 | 2.69588e-12 | 1.10541e-10 |
| D | 1.72508e-07 | 6.08247e-13 | 6.34728e-10 |
| Bd | 1.62317e-05 | 1.48231e-11 | 3.04153e-08 |
| Bs | 1.55101e-05 | 5.65737e-09 | 5.83004e-07 |

## 4.2 Canonical conversion and its conditions

Declare one canonically normalised fermion mode per cell, $c_x=a_0^{3/2}\psi(x)$, and $E_0a_0=1$ in natural units. The cell interaction $-E_0\kappa_H^{2}B^{T}KB/2$ then gives continuum coefficient $E_0a_0^{3}\kappa_H^{2}$. We use the empirical weak calibration $G_F=1.1663785\times10^{-5}$ GeV$^{-2}$ [12] to define $\varphi_H=(2\sqrt{2}G_F)^{-1/2}=174.103600$ GeV. The matching ansatz is

$$\kappa_H=\varphi_H/E_0,\quad C_i(E_0)=(\kappa_H^{2}/E_0^{2})c_i=(\varphi_H^{2}/E_0^{4})c_i. \tag{16}$$

The seed, source state and unit costs are fixed while $E_0$ changes. This is not a native continuum limit or physical renormalisation-group evolution of the Yukawa inputs. $E_0$ is a cell matching energy, not an independently identified mediator pole mass. Changing the mediator cost μ changes the source potential and may change its metric; a universal bound on $E_0\mu^{1/4}$ cannot be inferred by rescaling one coefficient while retaining the old state.

With the declared conversion, $E_0=1$ TeV corresponds to $a_0=1.9732698\times10^{-19}$ m and $t_0=6.5821196\times10^{-28}$ s. The source gap would then be 5.130994 TeV. These are coordinate and energy conversions under the matching ansatz. They do not identify a recording event rate, and the source gap is not a decay width. The native local-clock theorem [7] also requires a physical opportunity law and its attaching map.

## 4.3 Correlated kaon response and separate flavour diagnostics

For the kaon we evolve the simultaneous scalar coefficients with the corrected historical next-to-leading-order QCD matrices of [10], using its Landau-RI hadronic convention and rounded coefficients consistently.

The response is $M_{12}=P_2(C_2+\tilde{C}_2)+P_4C_4$. At 1 TeV, $P_2=-0.06308$ GeV$^3$ and $P_4=0.22385$ GeV$^3$; at zero degrees $M_{12}=(2.8031+0.9246i)\times10^{-18}$ GeV. The ratio of the magnitude of the sum to the sum of magnitudes is 0.99989. The contributions reinforce in every tested attachment.

$$b_{K,CP}=|\mathrm{Im}\ M_{12}|/(\sqrt{2}\,\Delta M_K|\varepsilon_K|),\quad b_{K,m}=|2\ \mathrm{Re}\ M_{12}|/\Delta M_K. \tag{17}$$

The budgets allow the new term to consume the entire historical measured magnitude, $\Delta M_K=3.483\times10^{-15}$ GeV and $|\varepsilon_K|=2.232\times10^{-3}$, without cancellation against the Standard Model. They are not confidence limits. The separate D, $B_d$ and $B_s$ $C_2$ comparisons use historical single-operator ceilings $1.6\times10^{-13}$, $7.2\times10^{-13}$ and $5.6\times10^{-11}$ GeV$^{-2}$ [9, Table IV]. Corresponding $\tilde{C}_2$ and $C_4$ checks are included in the package. These are separate screening comparisons, not a joint likelihood for a model with correlated coefficients.

**Table 6. Conditional scale crossings in TeV. The kaon uses correlated budgets; the last three columns use separate $C_2$ benchmarks.**

| ϑ | Kaon CP | Kaon mass | $B_d$ | D | $B_s$ |
|---|---|---|---|---|---|
| 0° | 0.530 | 0.192 | 0.909 | 0.425 | 0.303 |
| 60° | 0.690 | 0.229 | 0.929 | 0.450 | 0.319 |
| 120° | 0.758 | 0.260 | 0.910 | 0.418 | 0.325 |
| 180° | 0.560 | 0.266 | 0.854 | 0.457 | 0.318 |
| 240° | 0.687 | 0.247 | 0.811 | 0.475 | 0.302 |
| 300° | 0.744 | 0.208 | 0.854 | 0.405 | 0.291 |

The D and B columns use the 2008 single-operator ceilings. UTfit updated its new-physics analysis in 2021 [16, Fig. 3]. For a replacement $B_d$ ceiling L in the same operator and matching convention, the 60° crossing is 0.928792 TeV × $(L_{2008}/L)^{1/4}$, with $L_{2008}=7.2\times10^{-13}$ GeV$^{-2}$. At 1 TeV its budget is 0.744173 × $L_{2008}/L$. Equality occurs at $L\approx5.36\times10^{-13}$ GeV$^{-2}$, a tightening by a factor of 1.344. Any further tightening puts this row over budget at 1 TeV. A factor of just 1.045 already moves the flavour floor up to the 0.9391 TeV mass crossing. The fourth-root rule follows from (16) for a fixed coefficient ceiling. A contemporary comparison would need common-scale coefficients and, for the full model, correlated operator contributions and their phases. The kaon roots retain the scale-dependent evolution of Section 4.3.

The $B_d$ diagnostic is the largest of these crossings in every attachment. At zero degrees it gives 0.910848, 0.909205, 0.908408, 0.907859 and 0.907717 TeV as the inertia ranges over 0.04, $m_s$, 1, 16 and 256; the stationary mediator alone gives 0.908885 TeV. Thus its numerical stability is stronger than that of the mixing improvement. This robustness is conditional on the fixed seed and costs, not on arbitrary physical metric changes.

At zero degrees and $m_s$, write $A_\times$ for the cross-pair contribution to $c_2$ for $B_d$. For the mediator-only denominator $A_h$, $\mathrm{Re}(A_\times/A_h)=96.72\%$ and $|A_\times/A_h|=96.83\%$. With the full Table 5 coefficient in the denominator, including the connected source, the same ratios are 97.24% and 97.32%. Only the real projection is additive. The kaon is dominated by the 12 pair's own block, and cross-pair interference reduces its magnitude. At zero source displacement, scaling Ω by t makes $|c_2^{Bd}|/t$ approach $1.399238\times10^{-5}$, compared with $1.395055\times10^{-5}$ at t=1. This decomposition holds the state fixed.

# 5 The flavour preserving contact and metric dependence

Proposition 2 removes the identity contact from neutral flavour change, but not from all scattering or from mass response. With colour indices α,β, its four-fermion Lagrangian under the declared conversion is

$$\mathcal{L}_T^{(4)}=2C_T\Sigma_{f,i,j}(\bar{q}_{fLi}{}^{\alpha}q_{fRj}{}^{\alpha})(\bar{q}_{fRj}{}^{\beta}q_{fLi}{}^{\beta}),\quad C_T=\kappa_H{}^2/(\nu_T E_0{}^2). \tag{18}$$

The sum is within each up or down factor. Fierz rearrangement gives a colour-exchanged left-right vector product with coefficient $-C_T$; its colour-singlet and octet weights are 1/3 and 2, with $\mathrm{Tr}(T^aT^b)=\delta^{ab}/2$. It differs from the purely left-handed colour-singlet CMS benchmark [11]. At 0.91 TeV and unit $\nu_T$, $C_T=4.42\times10^{-8}$ GeV$^{-2}$, or twice that for the scalar form. Historical CMS left-handed scales of 12.8 and 17.5 TeV correspond to $2\pi/\Lambda^2=3.83\times10^{-8}$ and $2.05\times10^{-8}$ GeV$^{-2}$. Equal-magnitude crossings near 0.94–1.31 TeV are indicative only; neither the confidence limit nor the interference sign transfers to this operator.

The completion metric changes this comparison. If $X_H=\kappa_H T_H$ and the unit metric is assigned to $X_H$, then $\nu_T=\kappa_H^2$ and $C_T=1/E_0^2$. It is $1.21\times10^{-6}$ GeV$^{-2}$ at 0.91 TeV, with analogous magnitude crossings around 5–10 TeV. A collider conclusion requires the actual flavour, chirality and colour amplitudes, their QCD matching and the experimental likelihood. It also requires an ultraviolet description when partonic energies approach or exceed the cell matching energy; the low-energy contact cannot automatically be used throughout the dijet sample.

The same $C_T$ enters the instantaneous pole self-energy. In cell units its strength is $E_0^2C_T=\kappa_H^2/\nu_T$. It falls as $E_0^{-2}$ for unit T and equals one for unit $X_H$. This distinction determines whether the pole-mass budget can be met. The identity part cancels in neutral flavour change by Proposition 2 and in the first-order light-current ratio by Section 6.

The same distinction prevents identifying the reduced pion scale with the full flavour mediator scale. At $E_0=0.2259231807$ GeV, the formal fixed-seed conversion gives $|C_2^K|\approx1.34\times10^{-2}$ GeV$^{-2}$ and $|C_2^{Bd}|\approx1.89\times10^{2}$ GeV$^{-2}$. Those magnitudes cannot describe a small correction to measured flavour physics under this assignment. No perturbative low-energy QCD calculation is used to turn them into a precision exclusion. A separate derivation must relate any low two-flavour binding scale to the full construction.

## 6 Pole masses and the weak vertex in one regulator

Use the same leading matched $\bar{Y}_f$, derived source inertia and instantaneous kernel $K_{ct}=\nu_T^{-1}I+K_h$. Table 7 uses $\nu_T=1$. Let $\varepsilon_I$ multiply the instantaneous contact while leaving the source preparation and canonical seed fixed. The returned quantities are derivatives at $\varepsilon_I=0$. The source has already been averaged into $\bar{Y}_f$ and $K_h$; its retarded response $C_F$ is not inserted again as a static loop. This defines a controlled calculation in a specified restriction, not the full interacting self-consistent physical vacuum.

The free spatial quark Hamiltonian uses the inherited canonical Dirac symbol with cell spacing one and momentum p in $[-\pi,\pi]^3$. Its two helicity blocks have masses $\kappa_H\bar{d}_f$. Let $b_a$ be the 12×12 one-body scalar quadratures of the 36 completion coordinates and P the occupied negative-energy projector averaged over that cube. The symmetric-order self-energy functional is

$$S(Q)=\kappa_H^2\Sigma_{ab}K_{ct,ab}[-6b_a\mathrm{Tr}(b_bQ)+b_aQb_b],\quad \Sigma=S(P-I/2). \tag{19}$$

The direct trace includes three colours and two spins; exchange stays in the external colour and spin copy. Helicity balance fixes $P_{LL}=P_{RR}=I/2$ exactly. Cancelling that component analytically before quadrature avoids amplifying a tiny subtraction error through light-family eigenvalue differences. The pole-mass derivative is half the positive-minus-negative energy shift at rest, divided by $\kappa_H\bar{d}_{fi}$. It is a chirality-changing pole response, not the charging gap of a fixed-number finite cell.

For the temporal charged current $j=2q_{uL}^\dagger q_{dL}$ at zero spatial transfer, the occupied-to-empty response in the free energy basis is

$$\delta P(\omega)=\int_{\mathrm{cube}}d^3p/(2\pi)^3\,\Sigma_{\alpha\beta}|\alpha,p\rangle[(n_\beta-n_\alpha)j_{\alpha\beta}/(\omega-e_\alpha+e_\beta)]\langle\beta,p|. \tag{20}$$

$$\delta J_{W,ij}=\delta J_{W,\mathrm{legs},ij}+\langle u_i|S(\delta P(\omega))|d_j\rangle,\quad \omega=e_{ui}-e_{dj}. \tag{21}$$

$$R_{us/ud}=|J_{W,us}/J_{W,ud}|^2,\quad \delta R=2R\,\mathrm{Re}(\delta J_{W,us}/J_{W,us}-\delta J_{W,ud}/J_{W,ud}). \tag{22}$$

The first term in (21) contains the two external-state eigenvector derivatives generated by Σ. Keeping only those terms would omit a required vertex. In the two light channels the nonzero occupied-to-empty

denominators do not cross zero. Scalar and temporal-left vertices preserve helicity at this transfer, so the angular spin average is the average of the ±|p| blocks; the cubic momentum weights remain explicit. The calculation does not claim a general finite-momentum decay form factor or a prescription for open heavy-channel singularities.

The positive octant is partitioned into three pyramids $p=\pi r(1,s,t)$, with r,s,t between zero and one and normalised weight $3r^2$. The bulk current uses 20 and 32 Gauss-Legendre nodes per coordinate. An independently reduced mass integral uses 48 and 96 nodes. Finite Slater-determinant sums at periodic lengths 3, 9 and 33 reproduce both the external-state and vertex response with a single direct copy. The identity contact cancels from this first-order current while retaining a mass contribution, consistent with the finite identities in [1].

**Table 7. Detailed return at $\kappa_H=0.19$, $\vartheta=0$ and $E_0=916.335$ GeV. Entries are first derivatives, not finite-interaction predictions.**

| Quantity | Value | Scope |
|---|---|---|
| u c t mass derivatives | 0.104992 0.105020 0.086342 | Fractional pole derivatives |
| d s b mass derivatives | 0.083597 0.083602 0.087339 | Same cubic cutoff |
| $d\log(m_t/m_u)/d\varepsilon_I$ | −0.018651 | Ratio derivative |
| $R_{us/ud}$ | 0.053164963 | Unperturbed temporal current |
| $dR/d\varepsilon_I$ | $1.19709060\times10^{-5}$ | Legs $1.19734048\times10^{-5}$; vertex $-2.49876\times10^{-9}$ |
| $\lvert C_2^{Bd}\rvert$ | $6.98\times10^{-13}$ GeV$^{-2}$ | Historical separate ceiling $7.2\times10^{-13}$ |

At 916.335 GeV the largest mass slope is 10.50%, above the declared ten-percent budget. The zero-degree $B_d$ coefficient is already below its historical ceiling. Following the mass slope as the scale rises locates the threshold in Section 7.

## 7 The lower bound across all six attachments

Fix $E_0=1$ TeV, $\kappa_H=0.1741035997$, $m_s=18391/86955$ and $\mu=\nu_T=1$. Keep all six inherited attachments without optimising any mixing observable. For each, calculate both the instantaneous pole/current derivatives and the scalar flavour projections using the same matched seed. The kaon uses the correlated response of Section 4; D and B channels use all three separate historical operator checks. The ten-percent mass threshold below is an explicitly chosen perturbative budget, not an experimental confidence interval.

**Table 8. Unit T metric at 1 TeV. Mass and current columns are derivatives at $\varepsilon_I=0$. Flavour columns give fractions of the historical budgets.**

| $\vartheta$ | Max mass slope % | $10^5\,dR/d\varepsilon_I$ | $d\log R/d\varepsilon_I$ % | Kaon CP budget | Largest D or B budget |
|---|---|---|---|---|---|
| 0° | 8.82007 | +1.006174 | +0.01893 | 0.084095 | 0.683357 |
| 60° | 8.81999 | -0.856784 | -0.01607 | 0.234646 | 0.744173 |
| 120° | 8.81990 | -4.432262 | -0.08295 | 0.339315 | 0.686266 |
| 180° | 8.81994 | -6.154775 | -0.11525 | 0.103861 | 0.532682 |
| 240° | 8.81953 | -4.490932 | -0.08429 | 0.230745 | 0.432623 |
| 300° | 8.81984 | -0.918729 | -0.01728 | 0.314730 | 0.531617 |

With $\nu_T$=1, the mass-budget crossings lie between 0.939053 and 0.939082 TeV across the six attachments. At 1 TeV the maximum fractional mass derivative is below 0.08821. The largest relative current-ratio derivative in magnitude is below 0.001153. Each D or B budget is below 0.745 and the kaon CP fraction is below 0.340. The kaon mass fractions also fall below one. The current is a reported response. The mass budget and historical flavour ceilings set the lower bound.

Linearity of (19) allows the identity kernel and the mediator kernel to be contracted separately. Table 8a gives their contributions for each flavour at zero degrees. At this precision the identity shifts the light flavours alike. Its smaller top entry follows from the mass in the propagator. The largest mediator contribution over all six attachments is 1.931 percentage points. At zero degrees the slope of $\log(m_t/m_u)$ is −0.0156084. Across the six attachments its magnitude stays below 0.01565.

**Table 8a. Fractional pole-mass slopes at 1 TeV and $\vartheta$=0. Unit T entries are percentage points per unit $\varepsilon_I$. The last column gives the unit $X_H$ total in the same units.**

| Flavour | Identity on T | Mediator | Total on T | Total on $X_H$ |
|---|---|---|---|---|
| u | 6.889 | 1.928 | 8.818 | 229.209 |
| c | 6.889 | 1.931 | 8.820 | 229.211 |
| t | 6.847 | 0.409 | 7.257 | 226.308 |
| d | 6.889 | 0.130 | 7.020 | 227.411 |
| s | 6.889 | 0.131 | 7.020 | 227.411 |
| b | 6.889 | 0.445 | 7.334 | 227.725 |

For charm, which sets the 1 TeV maximum, 6.889 percentage points of the 8.820% slope come from the family-blind contact $C_T$ of Section 5. The mediator supplies the other 1.931 points. The 0.939 TeV crossing therefore mostly measures the contact common to the six flavours. The difference of mass slopes tests distortion of the hierarchy directly.

With the unit metric on $X_H$, only the identity column is multiplied by $1/\kappa_H^2$. Across all six attachments the resulting fractional mass slopes range from 2.263 to 2.292 at 1 TeV (226–229%). At high $E_0$ they tend to 2.273. Appendix A bounds the slopes throughout the range allowed by the historical flavour tests. No scale passes both sets of tests in this metric. The light current and the flavour-changing coefficients retain their values.

At zero degrees $dR_{us/ud}/d\varepsilon_l$=1.00617405×10⁻⁵. The external states contribute 1.00635496×10⁻⁵ and the vertex contributes −1.80913×10⁻⁹. Other attachments reverse the sign of the total (Table 8).

Figure 1 shows why the unit T result is one-sided. At fixed dimensionless seed the matched scalar coefficients fall exactly as $E_0^{-4}$, with additional QCD evolution in the kaon budgets. The instantaneous mass and light-current response is suppressed approximately as $E_0^{-2}$ in this regime. Table 4 is independent of $E_0$. All larger scales therefore remain available under the stated prescription. This scan describes a fixed-seed model with a fixed regulator and gives no physical upper bound.

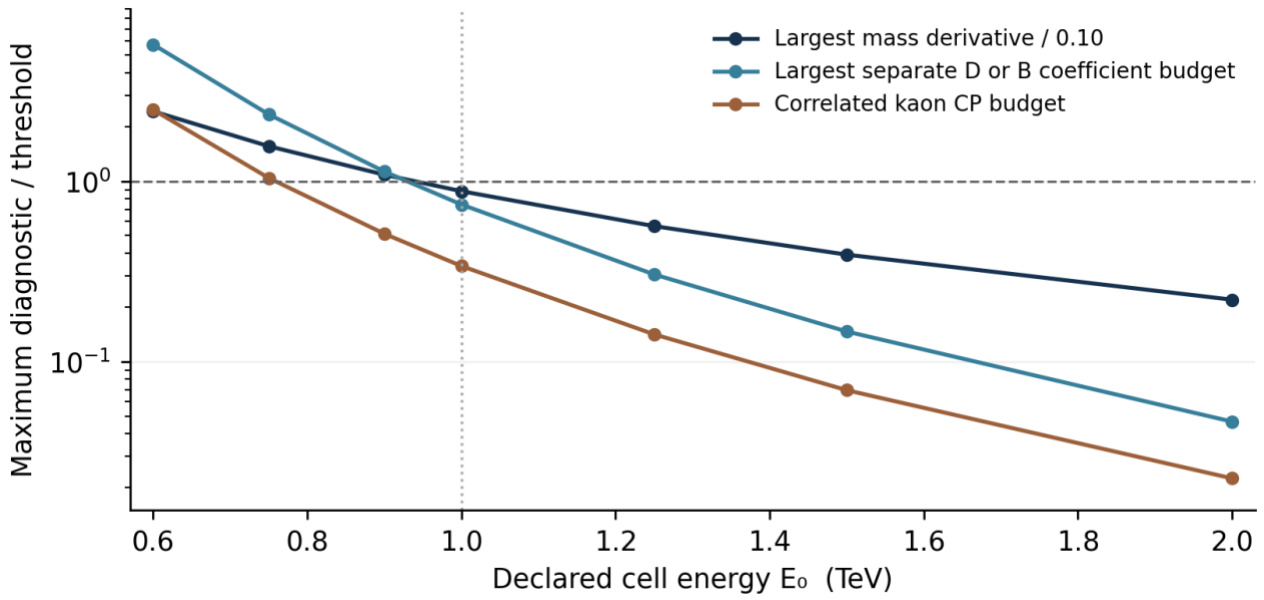



Figure 1. Unit T metric. Each point gives the largest diagnostic over the six attachments at that energy. The dashed line marks each diagnostic's threshold. The mass curve crosses last as the energy increases. The vertical line marks the 1 TeV example.

Quadrature changes from 20 to 32 nodes move the largest current-ratio derivative by less than $1.4\times10^{-12}$. The independent mass integrals at 48 and 96 nodes differ by less than $6.6\times10^{-9}$; comparison with the 32-node current implementation agrees within $8.5\times10^{-9}$. These differences are far smaller than the benchmark margins. They do not bound the omitted retarded-source loop, higher contact orders, ultraviolet matching, physical seed running or correlated experimental theory errors. In particular, a derivative below 0.10 does not bound the finite $\varepsilon_{I}=1$ remainder.

The lower bound uses the same mediator and source to evaluate neutral flavour change and mass response. The small light-current corrections leave the discrepancies in the leading CKM pattern unresolved. The physical weak current still requires the retarded source and matching to external particles.

# 8 Recording during the same finite dynamics

## 8.1 A specified channel and coherent propagation

The recording test retains the source explicitly, with one colour/helicity copy and seven fermions in twelve modes. We use the same drift attachment and inertia at $\kappa_H=1$ and at the 1 TeV coupling $\kappa_H=0.174103600$. Only the coupling is shared with the bulk calculation of Section 7. In each run the source spectrum is held fixed, the joint ground state is recalculated and the unit ordering interval is retained. The Hamiltonian is

$$H_{joint}=H_b\otimes I+\kappa_H\Sigma_a F_a(w)B_a-(\kappa_H^2/2)\Sigma_{ab}[I+K_h(w)]_{ab}B_aB_b. \tag{23}$$

The completion contact is exact at its Gaussian elimination, while the mediator contact uses the inherited local Gaussian and linear-Y restriction. The w dependence is retained. Its confining source potential and bounded finite-fermion coefficients give a self-adjoint, bounded-below Hamiltonian with discrete spectrum. Since w propagates explicitly, no extra $C_F(0)$ contact is added. These facts establish well-posed evolution of the finite construction; they do not identify its complete native physical history measure.

Use the resolved quark-doublet operation of [6] and fix its family rays in the coherent mediator frame $R_F=\mathrm{diag}(1,1,\zeta)F_3$, with $\zeta=\exp(2\pi i/3)$ and $(F_3)_{jk}=\zeta^{jk}/\sqrt{3}$. This basis is a declared attachment. The extension chooses one of the three rays equally and acts by number-preserving weak rotations of its left-handed doublet. Right-handed modes are spectators during the operation but interact under (23). For activity $\chi=1$ the one-doublet singlet and adjoint coefficients are $\alpha_{rec}=0.741581624$ and $\beta_{rec}=0.622146629$.

$P_{a,o}=n_{a,u}+n_{a,d}-2n_{a,u}n_{a,d}$, $Z_a=n_{a,u}-n_{a,d}$, $S_a^{+}=b_{a,u}^{\dagger}b_{a,d}$. (24)

$L_{a0}=I-(1-\alpha_{rec})P_{a,o}$, $L_{a1}=\sqrt{\nu_0}P_{a,o}$, $L_{az}=\sqrt{\nu_1}Z_a$, $L_{a\pm}=\sqrt{(2\nu_1)}S_a^{\pm}$. (25)

$\nu_0=1/6$, $\nu_1=0.094463343$, $\mathcal{E}_Q(\rho)=(1/3)\Sigma_{a,\mu}L_{a\mu}\rho L_{a\mu}^{\dagger}$. (26)

The coefficients obey $\alpha_{rec}^2+\nu_0+3\nu_1=1$. Empty and doubly occupied doublets are singlets; the singly occupied sector is the corresponding isotropic two-state channel. Completeness, unitality and number conservation follow, and its one-particle restriction recovers the resolved-Q operation. This local Fock extension is specified explicitly; other collective extensions are not asserted equivalent. The finite current is $J_W=2\Sigma_a S_a^{+}$, and the initial state is the lowest joint state in the $(N_u,N_d)=(3,4)$ sector.

For a unit ordering interval let $U(t)=\exp(-iH_{joint}t)$ and $A(t)=-i\int_0^t U(t-s)J_W U(s)ds$. Inserting one completed operation at $\tau$ gives the branch amplitude

$A_{a\mu}(1,\tau)=[U(1-\tau)L_{a\mu}A(\tau)+A(1-\tau)L_{a\mu}U(\tau)]/\sqrt{3}$, (27)

$\mathcal{R}_Q(\tau)=\Sigma_{a\mu}\|A_{a\mu}(1,\tau)|i\rangle\|^2$, $P_{probe}=\varepsilon^2\mathcal{R}_Q+O(\varepsilon^4)$. (28)

The amplitudes before and after the operation interfere within each retained branch before squaring. Every required charge sector is propagated, with no projection back onto a preferred sector and no division by survival probability. Trace preservation proves the final-endpoint identity $\mathcal{R}_Q(1)=\mathcal{R}_0$. It does not remove an intermediate operation. At $\kappa_H=1$ with sixteen source states $\mathcal{R}_0=0.932311980$, while an initial operation gives 0.931459388 and a midpoint operation 1.136109635. Source enlargement to twenty-two states changes those last two coefficients by approximately $10^{-9}$.

## 8.2 Equal work does not specify the response

At $\kappa_H=1$ on the stationary preparation a full Q operation supplies work $W_Q=0.964391958$ in construction energy units. To separate its structure from a direct change of the observed left occupancy, use $U_R=\exp(i\pi N_R)$, with $N_R$ the total right-handed occupation. It preserves every left occupation and intertwines the charged current across the required sectors. Three right-family exchanges and common right phases $\pi/2$ and $\pi$ were checked for work before computing their probe response. The $\pi$ phase supplies the largest work among those five fixed candidates; this is not an optimisation over all unitaries or a physically selected recording rule.

$W_R=0.496120370$, $\lambda_Q=W_R/W_Q=0.514438518$, $\mathcal{E}_{diluted}=(1-\lambda_Q)Id+\lambda_Q\mathcal{E}_Q$. (29)

A mixture of this right phase with the identity cannot supply the full Q work: it would require probability 1.94387. The comparison therefore uses the lower common work in (29). Work equality holds on the stationary preparation, at zeroth order in the probe, rather than as an operator identity on arbitrary states. The source and Hamiltonian are unchanged.

**Table 9. Unit coupling, sixteen source states. Changes relative to the unrecorded pulse at equal work 0.496120370.**

| Insertion $\tau$ | Diluted Q readout | Right-only phase |
|---|---|---|
| 0.0 | -0.047045% | +67.974506% |
| 0.5 | +11.245309% | +28.567676% |
| 1.0 | 0 | 0 |

At $\kappa_H=1$ the two midpoint increases are 11.245309% and 28.567676%. The right-phase response develops during propagation even though the operation preserves the left-handed occupancy. The ten- and sixteen-state pulse coefficients agree within $7.3\times10^{-8}$.

### 8.3 Equal work at the benchmark coupling

At $\kappa_H$=0.174103600 the order of the two work costs reverses. The full Q readout supplies $W_Q \approx 0.033154$, while right parity supplies $W_R \approx 0.276602$. Equal work on the initial ground state now requires the full Q readout and a mixture applying right parity with probability $W_Q/W_R \approx 0.119861$. The undiluted right phase is also shown so that its coupling dependence can be compared directly.

**Table 9a. Benchmark coupling, sixteen source states. Percent change from the unrecorded pulse. The middle pair has equal work $W_Q$. The last column shows the full right phase at its own work.**

| Insertion τ | Full Q | Diluted right phase | Full right phase |
|---|---|---|---|
| 0.0 | -6.32974% | -0.03141% | -0.26204% |
| 0.5 | -7.86995% | +0.00194% | +0.01615% |
| 1.0 | 0 | 0 | 0 |

The unrecorded pulse coefficient is 10.78575. The inclusive strength of the unrecorded initial state, $\|\|J_W|i\rangle\|\|^2$, is 10.81118, so the unit-duration pulse samples about 99.76% of that strength. At the midpoint the full Q operation suppresses the pulse by 7.870%, while the equal-work right mixture changes it by +0.00194%. Both operations recover the unrecorded endpoint. At ten states a separate spectral sum gives inclusive strengths of 11.92794 at unit coupling and 10.81118 at the benchmark coupling. The contrast survives at the benchmark coupling, with a reversal of the Q response and a much smaller right-only effect. The finite calculation concerns the response conditional on one operation.

Increasing the source cutoff from ten to sixteen changes each tabulated shift by less than $10^{-8}$ percentage points.

### 8.4 The occurrence law and the energy source

For a homogeneous independent-event control with small mean count $n_{rec}$, the conditional time of one event is uniform and the response is $\mathcal{R}(n_{rec})=\mathcal{R}_0+n_{rec}\int_0^1[\mathcal{R}_Q(\tau)-\mathcal{R}_0]d\tau+O(n_{rec}^2)$. At $\kappa_H$=1 the calculated coefficient is 0.114192, or relative slope 0.122483 per expected completed operation. This is a response available to an event law, not a derivation of that law. A state- or history-dependent process needs its corresponding weighted instrument.

A record is implemented by a dilation that appends a new label and preserves earlier labels. Its reduced channel alone does not specify the Hamiltonian, state or energy reserve of the recording environment. In particular, a passive energy-releasing weak decay and this positive-work Q operation cannot be identified by giving them the same event count. The common event-weighting framework [13] requires the operation, energy exchange and occurrence law to be included together. The energy supplied by (29) is therefore not silently converted into a measured lifetime.

## 9 From a cell response to a physical particle

The finite cell has definite quantum numbers that determine which particle interpretations are possible. For example, with normal ordering relative to three occupied modes of each species in the finite cell, baryon number is $(N_u+N_d-6)/3$. The (3,4) preparation and (4,3) final sector both have baryon number 1/3. They cannot be called a pion. A charged meson-like sector is (4,2), with baryon number zero; colour singlet, spin, parity and a stable pole must also be returned. A change of energy units cannot supply those quantum numbers.

Eliminating configurations requires transforming the current with the states. Let P retain a sector, Q=I−P and $G_E=(E-QHQ)^{-1}$ below the eliminated threshold. The injection, self-energy and induced norm are

$$W_{inj,E}=P+QG_EQHP,\quad \Sigma_P(E)=PHQG_EQHP,\quad N_E=W_{inj,E}^{\dagger}W_{inj,E}=P-\Sigma_P'(E). \tag{30}$$

$$J_{W,phys}=N_f^{-1/2}W_{inj,f}^{\dagger}J_WW_{inj,i}N_i^{-1/2}. \tag{31}$$

Proposition 3. If a flavour generator T commutes with H and P, its equal-energy matrix element under (31) is T on the retained multiplet. Proof. The resolvent intertwines T, so $W_{inj}T=TW_{inj}$ and $W_{inj}^{\dagger}TW_{inj}=NT$; N also commutes with T. Multiplication by $N^{-1/2}$ on both sides proves the statement. The identity $N=P-\Sigma'$ follows from $dG_E/dE=-G_E^2$. ▫

This exact charge recovery includes entangled dressing. It explains why an isolated change of mass eigenvectors or a projected current $PJ_WP$ generally cannot replace the dressed response. It does not determine an axial vacuum-to-pion overlap. The latter requires a common bound-state pole and a consistently matched irreducible interaction, as in the axial-identity condition of [14]. Matching a measured pion mass while importing its axial overlap is a recovery check using external hadron data, not a VERSF pion prediction.

The scalar contact, retarded colour and compact-field binding investigations motivate a separate low-energy matching requirement. Their useful acceptance quantities are a stable pole, its mass dependence and its axial residue in the same regulator. A small box may retain a residual chiral gap [15], so volume and quark-mass dependence must be tested together. Those investigations do not justify identifying their low scale with the full flavour mediator, as Section 5 shows. The bound-state problem is retained as an open physical interface independently of the illustrative 1 TeV reference.

## 10 What this adds to the Standard Model derivation

The published mediator paper [1] established a mechanism for modifying quark mixing. This calculation gives the source a specified dynamics, derives its time-dependent response and uses the resulting quark interactions to constrain the cell energy. The ten-percent mass budget and historical flavour comparisons admit $E_0\gtrsim0.9391$ TeV for unit T. The family-blind contact sets most of that floor. Unit $X_H$ gives no admissible energy. These results identify the completion metric as a physical input that a derivation of the quark sector must fix.

At the benchmark coupling the Q readout and right phase differ even after their mean work is matched. That comparison isolates information about the operation beyond the energy it supplies. Deriving a physical event rate still requires its environment and occurrence law. The next mass and current calculations require the retarded source contribution on the same canonical external states.

**Table 10. Requirements for the next complete physical return.**

| Required object | Where it enters | Acceptance test |
|---|---|---|
| Retarded source self-energy and vertex | $C_F(\omega)$ with the same external states | Recover Section 6 when the retarded coupling is removed; preserve charge identity |
| Physical carrier and metric | Source embedding, drift attachment and completion cost | Recover the static action and the derived metric together; state any extra cross blocks |
| Scale and running | $E_0$, canonical fields, inherited Yukawa seed | Use one declared scheme, thresholds and electroweak matching for masses and flavour |
| Correlated experimental comparison | All scalar coefficients and their phases | Include Standard Model amplitudes, hadronic uncertainties and a joint likelihood |
| Record operation and occurrence | Channel, environment energy and event law | Recover the finite channel and endpoint identity; supply the physical energy reserve |
| A physical bound state | Common pole and weak residue | Return quantum numbers, mass/volume dependence and the matched axial response |

The dynamical source, the metric-dependent lower bound and the two-coupling recording comparison extend the stationary mixing calculation. The remaining tests concern physical scale matching, a joint flavour comparison and the complete weak current. The leading mixing pattern still misses measured CKM entries.

## Appendix A Numerical conventions and independent checks

The source calculation uses a two-dimensional Hermite basis with 24 and 32 functions per real coordinate and quadrature order N+8. Source eigenvectors, rather than independent stochastic noise samples, generate every source mean and spectral covariance. The real mediator basis is $\xi_h=\sqrt{2}(\mathrm{Re}\ h,\mathrm{Im}\ h)$, and the completion vector stores all real entries followed by all imaginary entries. The scalar coefficients use bilinear transposes. The kaon phase convention is fixed before comparison; conjugating the full attachment changes all CP-odd signs together.

The historical kaon implementation uses the corrected evolution coefficients of [10, Eqs. (6)–(10)], $\alpha_s(M_Z)=0.119$ and top threshold 175 GeV, retaining its hadronic inputs and scheme together. Matching is tree level and evolution is NLO; scheme uncertainty of the omitted matching remains. The D and B roots use the fixed 2008 ceilings of [9]. The kaon roots retain the scale dependence of $P_2$ and $P_4$.

Metric control. Let $d_i$ be a matched singular value and define $I_i(\kappa)=\langle 1/\sqrt{(|p|^2+\kappa^2 d_i^2)}\rangle$, the normalised cubic average. Inserting the identity kernel into (19) gives the fractional slope $6(\kappa^2/\nu_T)I_i$. For unit $X_H$ the explicit $\kappa^2$ cancels. As $\kappa\to 0$ this expression tends to $6\langle 1/|p|\rangle=2.272806$, while the mediator contribution vanishes. The mild mass dependence of $I_i$ explains the small flavour variation of the identity column in Table 8a.

A bound covers the interval between the 1 TeV example and the high-energy limit. By linearity of (19), write the mediator slope of flavour i as $\kappa^2\Sigma_j M_{ij}I_j$, where $M_{ij}$ is the contraction with only singular mode j retained in the off-diagonal projector, divided by $d_i$. The companion code evaluates these fixed coefficients for all six attachments. The largest absolute row sum is below 1.692. For $E_0\geq 0.800$ TeV, $\kappa\leq\varphi_H/(800\ \mathrm{GeV})$, $|p|\leq\sqrt{3}\pi$ and $I_j\leq\langle 1/|p|\rangle\leq 3/(2\pi)$ by the radial pyramid coordinates. Subtracting the resulting upper bound on the mediator magnitude from $6/\sqrt{(3\pi^2+\kappa^2 d_i^2)}$ leaves every unit $X_H$ slope above 1.06, well above 0.10. Below 0.800 TeV every attachment already exceeds its historical $B_d$ ceiling (Table 6).

**Table 11. Numerical checks and their practical meaning.**

| Check | Observed discrepancy | What it verifies |
|---|---|---|
| Source embedding and static recovery | Below $1.4\times10^{-15}$ | Metric elimination and recovered static coefficients |
| Identity contact in random mass frames | Below $2.5\times10^{-16}$ | Exact neutral-flavour cancellation |
| Symmetric unprepared mediator | Below $4.6\times10^{-19}$ | Threefold-symmetry cancellation |
| Finite Slater versus response current | Below $5.6\times10^{-13}$ | Independent first-order vertex and external-state algebra |
| Unit T bulk current 20 to 32 nodes | Below $1.4\times10^{-12}$ | Quadrature stability for every attachment |
| Unit T pole integrals 48 to 96 nodes | Below $6.6\times10^{-9}$ | Mass quadrature stability |
| Unit-coupling right control 10 to 16 | Below $7.3\times10^{-8}$ | Finite recorded-cell convergence |
| Unit-coupling equal-work mismatch | Below $5.6\times10^{-17}$ | Matched work on the stationary preparation |

An independent mass contraction at the 1 TeV point agrees with the current implementation to better than $8.5\times10^{-9}$. The positive momentum weights sum to one, and the analytic helicity subtraction is carried out

before integration. The source-space, bulk-quadrature and historical-input errors are distinct. The reported tolerances establish reproducibility of the restricted calculation; they do not turn the fixed regulator into a continuum result.

## Appendix B Reproduction and source provenance

The companion package Physical_Scale_and_Weak_Response_Calculation.zip contains the fixed seed, local dependency subset, forward solvers, complete numerical rows, a methods note and a SHA-256 manifest. The direct public baseline is [1], dated 24 November 2026; its 25-page PDF is the reference for the division of contributions in Table 2. Public source papers [2–7] supply the ledger, residual forms, radial completion, history and weak-current conventions. Their relevant statements are used at their stated conditional grade; this paper does not claim to rerun every primitive source execution.

source_motion.py checks the wheel embedding and returns the induced metric and spectral covariance. meson_consistency.py returns all six matched frames, kernels, phase-fixed scalar coefficients and historical kaon evolution. attachment_diagnostics.py tests inertia dependence, symmetric cancellations and pair-block attribution. common_point_response.py checks the current vertex against the independent Slater-determinant implementation. joint_scale_test.py returns all six common-scale rows, the mass-budget crossings and Figure 1 data. right_handed_control.py returns the fixed right-only candidates and the lower-work comparison. metric_response.py returns the mass split and interval bounds. benchmark_recording.py propagates both recording operations at the benchmark coupling and compares them at equal work. The README gives the reproduction commands.

The seed masses and $\Omega$ are inherited inputs, $G_F$ is an empirical normalisation, and the historical flavour comparisons are diagnostic data. The 1 TeV reference and ten-percent derivative budget are declared choices. No experimental CKM target enters the forward source, loop or recording solvers. The original favourable attachment was already known when the mediator family was constructed [1]; keeping every attachment here does not make that history blind. The package is supplied with this manuscript. No public repository or DOI is claimed before deposition.

## References

[1] Keith Taylor. A History Mediator for Quark Mixing in VERSF. Stationary, Quantum and Interacting Tests. 24 November 2026. Published baseline, 25 pages. Source

[2] Keith Taylor. VERSF Standard Model Derivation Ledger November 2026. 18 November 2026. Pages 14–15. Source

[3] Keith Taylor. The VERSF Master Substrate Action and Constitutive Descent Theorem. July 2026. Sections 17–21 and 47F. Source

[4] Keith Taylor. The VERSF History Measure Generation Geometry and Branch Closure Theorem. July 2026. Sections 31–38 and 56A. Source

[5] Keith Taylor. Bounded Fold Dynamics and the Particle Spectrum in VERSF. 16 November 2026. Section 9.3 and Proposition 13. Source

[6] Keith Taylor. The Physical Weak Current and Quark Mixing in VERSF. November 2026. Sections 7–12. Source

[7] Keith Taylor. The Sequential Opportunity to Lorentzian Commitment Time Attaching Map in VERSF. September 2026. Source

[8] A. Ceccucci, Z. Ligeti and Y. Sakai. CKM Quark Mixing Matrix. Particle Data Group, 2025 update. Source

[9] M. Bona et al. UTfit Collaboration. Model independent constraints on ΔF=2 operators and the scale of New Physics. Journal of High Energy Physics 03 (2008) 049. Table IV. Source

[10] M. Ciuchini et al. $\Delta M_K$ and $\varepsilon_K$ in SUSY at the Next to Leading order. Journal of High Energy Physics 10 (1998) 008. Corrected arXiv version 2, 29 March 2000. Source

[11] CMS Collaboration. Search for new physics in dijet angular distributions using proton proton collisions at √s=13 TeV and constraints on dark matter and other models. European Physical Journal C 78 (2018) 789. Author-name erratum: 82 (2022) 379. Source

[12] Particle Data Group. Electroweak Model and Constraints on New Physics. 2025 review, Section 10.3.2. Weak normalisation input. Source

[13] Keith Taylor. Completed Event Weighting and Force Response in VERSF. November 2026. Sections 10–13 and 15. Source

[14] H. J. Munczek. Dynamical Chiral Symmetry Breaking, Goldstone's Theorem and the Consistency of the Schwinger Dyson and Bethe Salpeter Equations. Physical Review D 52 (1995) 4736–4740. Source

[15] W. Bietenholz et al. QCD in the δ Regime. AIP Conference Proceedings 1343 (2011) 321–323. Source

[16] M. Bona et al. UTfit Collaboration. Unitarity Triangle global fits beyond the Standard Model: UTfit 2021 new physics update. PoS EPS-HEP2021 (2022) 500, Fig. 3. Source